Journal of Magnetism and Magnetic Materials 322 (2010) 858–865

Contents lists available at ScienceDirect

Journal of Magnetism and Magnetic Materials

journal homepage: www.elsevier.com/locate/jmmm

Near-Curie magnetic anomaly at the Ni/C interface observed by electron holography

Loris Ferrari [a], Giorgio Matteucci [a], Marvin A. Schofield [b], Marco Beleggia [b,*,1], Yimei Zhu [b]

[a] Department of Physics, University of Bologna, V.le B. Pichat 6/2, 40127 Bologna, Italy
[b] Brookhaven National Laboratory, Building 480, Upton, NY 11973, USA

ARTICLE INFO

Article history:
Received 15 September 2009
Received in revised form
6 November 2009
Available online 22 November 2009

PACS:
61.05.jp
74.25.Ha
77.80.Bh
75.30.Gw

Keywords:
Electron holography
Curie temperature
Nickel film
Surface anisotropy
Spin-reorientation transition

ABSTRACT

We analyze with electron holography carried out in a transmission electron microscope the near-Curie behavior of magnetism at the edge of a Nickel thin film coated with Carbon. In-situ experiments with finely controlled variations of the sample temperature reveal an anomaly in the ferromagnetic to paramagnetic phase transition when the film temperature is a few degrees above the nominal Curie point. We interpret the anomaly as a strain-induced spin reorientation transition triggered by the differential thermal expansion of Carbon and Nickel. We present a model that quantitatively reproduces the main features of the observed signal. The model is developed in terms of an anisotropic, temperature dependent exchange coupling between the Nickel moments at the Carbon interface that favors their vertical alignment at low temperatures.

© 2009 Elsevier B.V. All rights reserved.

1. Introduction

Electron holography (EH) carried out in a transmission electron microscope (TEM) is a powerful technique [1] for the microscopic analysis of magnetic samples down to a spatial resolution in the range 1–5 nm accompanied by sensitivity to magnetic flux down to a tiny fraction (~ 0.01) of the flux quantum. EH has been widely employed in recent years for studying magnetism at the sub-micron scale in its many forms, for example, in characterization of the domain structure in magnetic thin films [2,3], measurement of domain wall widths [4] and magnetic vortices [5,6], induction mapping in arrays of nanoparticles [7–9], and study of magnetic behavior in nanopatterned arrays and individual magnetic elements [10].

In the current study, we use EH to examine the magnetic properties as a function of temperature of Nickel films coated with a few nm's of carbon to prevent oxidation, increase structural stability and reduce electron beam induced charging. We focus our attention within a single Weiss domain, a region of about 1 μm^2 size. We measure the magnetization from room-temperature to just above the critical temperature T_c at which the spontaneous magnetization would vanish when no field is applied.

EH is an interferometric approach that relates the phase modulation of the electron wavefront $\varphi(x,y)$ to the local magnetic field $\mathbf{B}$ (measured in Tesla) in the sample. Specifically, assuming that (i) stray fields are absent, (ii) the field in the sample does not depend on z, and (iii) the sample thickness t is constant, the phase gradient is related to the magnetic field by

$$\vec{\nabla}\varphi(x,y) = \frac{\pi t}{\phi_0}[B_y(x,y)\hat{\mathbf{x}} - B_x(x,y)\hat{\mathbf{y}}], \quad (1)$$

where $\phi_0 = 2.07 \times 10^{-15}\,\mathrm{T\,m^2}$ is the flux quantum, and $\hat{\mathbf{x}}$ and $\hat{\mathbf{y}}$ are the unit vectors of the chosen reference system in the sample plane. Hence, the variation of the phase slope with temperature is a direct measure of the temperature-dependent local magnetic field.

In view of any advanced experiment using EH, aiming, for instance, to study the critical exponents or size effects on magnetic transitions, it is necessary to understand experimental limitations and constraints inherent to sample preparation and quantification of the technique, the influence of the TEM on measured quantities, and, in fact, the detailed nature of the sample on interpretation of any observed behavior.

* Corresponding author.
E-mail address: mb@cen.dtu.dk (M. Beleggia).
[1] Now at: Center for Electron Nanoscopy, Technical University of Denmark, DK-2800 Kgs. Lyngby, Denmark

0304-8853/$ - see front matter © 2009 Elsevier B.V. All rights reserved.
doi:10.1016/j.jmmm.2009.11.017

For example, magnetic lenses in the TEM may leave a residual field $\mathbf{B}_{res}$ acting on the sample. For the microscope used in our experiments, a JEOL 2100F [11] we have measured a residual field of 0.16 mT in the plane of the sample and 0.4 mT along the beam direction, perpendicular to the sample plane [12]. This limits the possibility of measuring the precise vanishing of the magnetization at, and above, the Curie temperature of the sample.

In terms of the technique itself, dynamical contribution to the measured electron phase shift, the field of view, and the acquired signal-to-noise ratio (SNR) are always elements to consider in any EH experiments. In particular for a temperature study, single crystal samples are extremely problematic since the precise diffracting conditions of the sample strongly influence the dynamical contributions to the phase shift. In order to minimize the undesired dynamical effects, it is standard to orient a single-crystal sample to a weakly diffracting condition. As the sample temperature is changed, however, it is invariable that precise orientation of the sample would change unpredictably due to thermal expansion. Hence, we carried out our experiments with a polycrystalline film, with an average grain size of about 10 nm. While dynamical effects might still be present in individual grains, those that are oriented by chance along a strongly diffracting direction, it is easy to identify such regions and exclude them from detailed analysis.

Additionally, in order to avoid electron absorption and loss of detection sensitivity during hologram recording, the sample thickness cannot be larger than a few tens of nanometers. On the other hand, a thicker sample provides a stronger signal thereby improving the SNR. To balance high detection sensitivity with high SNR, deposited samples of suitably chosen thickness are, therefore, the best candidates for EH measurements, having also the added benefit of uniform thickness.

Thin films (few nm thick) are currently used with other techniques [13–15] to test the existing renormalization group theories of magnetic transitions in 2-dimensions. In this work, we analyze relatively thick films (50−60 nm), that are expected to display a marked 3-dimensional character. Our original aim for this endeavor was to study magnetism of a pure Ni film near the Curie point in order to test the ability of EH to measure the critical behavior and in particular the critical exponents for a quasi-3D system such as our Ni film. However, while carrying out the experiments, we observed an unexpected anomaly in the magnetization signal above nominal T_c, and we are here reporting on this phenomenon and on our interpretation of it.

2. Experimental results

Nickel films for TEM sample preparation were grown at room temperature by UHV electron-beam evaporation on single-crystal NaCl substrates. The films used in this study were grown to a nominal thickness of 60 nm, and were polycrystalline in nature with roughly 10 nm grain size. The films were capped with 2 nm amorphous Carbon to prevent oxidation, increase structural stability of the films and to reduce electron beam-induced charging. TEM samples were finally prepared by dissolving the NaCl substrate in de-ionized distilled water and floating fragments of the film onto standard Cu TEM grids. We did not expect measurable effects of the Carbon cap on the magnetic properties of the sample, but, in fact, we found that such procedure may have dramatic effects as it is described momentarily.

The experimental EH arrangement used to observe and measure the magnetic distribution in our Ni films is schematically represented in Fig. 1. For simplicity, the electron optical system of the microscope has not been illustrated (for details, see Ref. [16]). Referring to the figure, a coherent electron beam (EB) illuminates

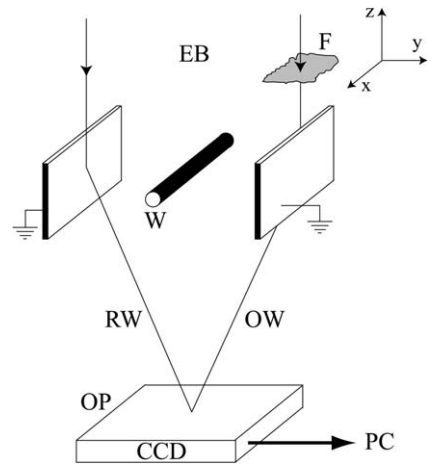

Fig. 1. Sketch of the setup for electron holography experiments.

an edge-region of a Ni film (F). One part of the beam is transmitted through the Ni foil while the remaining part is transmitted through the adjacent vacuum region. The two beams propagate towards an electrostatic biprism, which consists of a thin conducting wire (W) placed between two grounded plates. When a positive potential is applied to the wire, an electrostatic field arises that deflects the two beams to overlap, leading to coherent interference in the observation plane (OP). The recorded interference pattern, referred to as an off-axis hologram, contains information about the relative phase shift between the object wave (OW) and the reference wave (RW). The hologram is recorded with a slow-scan CCD camera and digitally processed using Fourier techniques [16] to reconstruct the complex image wave (amplitude and phase with respect to vacuum) associated with an observed sample region. As described by Eq. (1) in the introduction, the reconstructed phase shift is quantitatively related to the thin film thickness and magnetic field distribution in the sample. While quantitative measurements in this study are made directly from the recovered phase shift, visualization of contour lines that can be directly interpreted as projected magnetic flux lines is obtained by presenting the cosine of the phase shift.

Fig. 2(a) shows an off-axis hologram of a portion of the Ni film. The sample is located in the left side of the image, with the sample edge running vertically. The right side of the hologram is the adjacent vacuum region. Fig. 2(b) reports the cosine map of the sample at a temperature of 627 K. The black and white fringes represent magnetic flux lines. Since the cosine map in Fig. 2(b) was amplified three times (i.e., the image displays the quantity $1+\cos[3\varphi(x,y)]$), between two adjacent fringes, marked A and B, a phase shift of $\pi/3$, and hence a third of a quantum of magnetic flux ($\phi_0/3$), is enclosed. As expected, by increasing the specimen temperature the magnetization decreases so that a smaller number of fringes is observed, as shown in Fig. 2(c) where the temperature has been brought up to 702 K. The finer fringes observed at the edge of the film in both Figs. 2(b) and (c) are due to the rapid increase in sample thickness. Measurements are always made away from the edge region where the film has uniform thickness.

Many EH experiments were conducted from different areas of several different samples. In each experiment, regions of the sample were identified where the film edge was straight over the field of view and where the room-temperature magnetic domain configuration was parallel to the sample edge. This configuration was ideal for performing EH experiments, which require a nearby vacuum region for the reference wave, and provided a stable

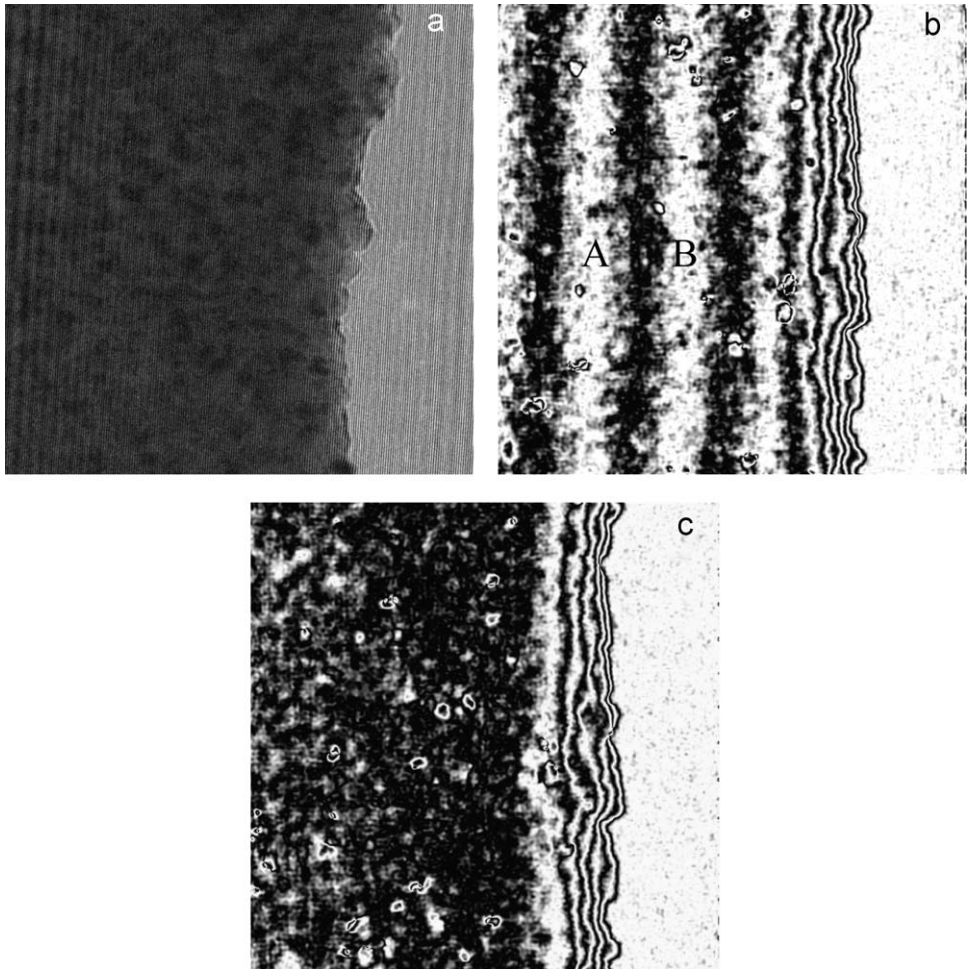

Fig. 2. (a) Electron hologram of the Nickel film; (b) reconstructed phase, displayed as a 3× amplified cosine map, at a temperature of $T = 627$ K; (c) reconstructed phase at $T = 702$ K.

domain configuration from which to measure the decrease in magnetization as a function of increased temperature. In each experiment, holograms were recorded with about 2.4 nm interference fringes having $\sim 30\%$ contrast in vacuum and $\sim 14\%$ contrast in the sample. A reference hologram was also recorded at each temperature step, and utilized during phase reconstruction to minimize distortions from the imaging system.

Ten temperature-dependent holography experiments were conducted, several being only partially successful due to equipment or sample failure. Indeed, a complete temperature series, e.g., as shown in Fig. 3, took 12–16 h to record. The lengthy time to conduct the experiment was to ensure thermal equilibrium at every temperature step, and to probe the magnetization behavior as finely as possible near the Curie temperature. For the series shown in Fig. 3, 40 data points were accumulated, including stepping the temperature by about 1° at the finest sampling in the crucial range near the transition temperature. A Gatan Smartset temperature stage was used to control the sample temperature, and increments were made by stepping the resistive current of the stage control rather than setting a target temperature. We found this procedure crucial to obtaining a true thermal equilibrium of the sample since setting a desired temperature through the control box invariably caused temperature oscillations (roughly by 1°) as the power supply cycled current in order to maintain the target temperature. While holding the sample temperature $\pm 0.5°$ is suitable for most applications, it was not sufficient for our experiments. Object and reference holograms were recorded only after all thermal drift had dissipated, which was typically about 5–10 min after the finest temperature increments, but was up to an hour or more for the larger steps.

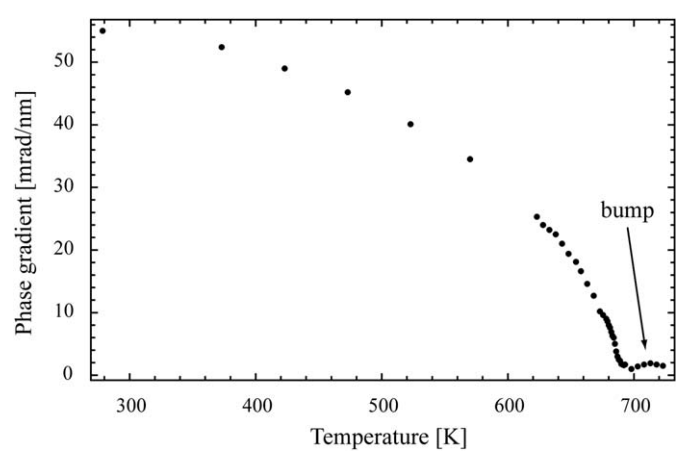

Fig. 3. Measured signal from electron holography. The measured phase gradient may be converted to magnetization (measured in Tesla) according to $\phi_0 \nabla\varphi = \pi t \mathbf{M}(T)$, where t is the nickel foil thickness.

The phase gradient (i.e., local magnetization) was measured from each reconstructed hologram pair (object and reference) as a function of temperature as follows. First, each hologram was pre-

processed for noise reduction [17] and then reconstructed according to standard Fourier means [16]. The pre-processing for noise had a two-fold benefit. While it reduced the interpretable spatial resolution in the recovered phase shift, it allowed for much more accurate measurement of the phase gradient. The noise filtering also reduced artifacts associated with low-contrast regions due to random crystallites of the sample being oriented in strongly diffracting conditions.

After phase reconstruction, the vacuum region of each phase map was checked to be flat indicating that long-range fringing field did not perturb the reference wave and that the reconstruction was faithful and reliable for magnetization measurement. A $220 \times 400\,\mathrm{nm}^2$ region (roughly 60 nm from the sample edge) was identified to be present in each phase map of the entire temperature series, and a preliminary phase gradient was measured by (least-squares) fitting a plane to this region of interest. The difference between the fitted plane and the reconstructed phase map indicated regions where dynamic effects contributed locally to the recovered phase shift due to random crystals oriented in strongly diffracting conditions. This difference map was used to create a mask that was further used to refit a plane to the reconstructed phase, but by excluding the regions known to be affected by local diffraction artifacts. The gradient of the final fitted plane was finally used as our measured phase gradient (or relative magnetization) at each temperature step. Based on the goodness-of-fit, reproducibility, and small residual deviation from linearity, we conservatively estimate our measurement sensitivity to be less than 1 mrad/nm.

Fig. 3 summarizes measurements from one temperature-dependent holography experiment. The results are consistent with additional experiments performed on different regions of the same sample, as well as different samples, where all features of Fig. 3 were reproduced. As shown in Fig. 3, the measured magnetization reaches a minimum, then increases again exhibiting a small but significant bump. This feature cannot be attributed to experimental errors, as it is well above the phase sensitivity of our measurements.

3. Analysis

In deposited magnetic film samples the bulk magnetic moments lie in the easy plane of deposition (x,y), with ferromagnetic correlations only. Actually, the present experiment measures the in-plane magnetization alone, as no interaction is in effect between off-plane fields and the electron beam. Since thermal energy tends to destroy the magnetic alignment, the intensity of the *total* spontaneous magnetization is expected to decrease with increasing temperature, in the absence of ferrimagnetic effects. Therefore, a ferromagnetic system like Ni leaves us with very few possible explanations for the bump displayed in Fig. 3, the most reasonable of which is that a relatively small fraction of magnetic moments, which are oriented along the z-axis at low temperature, rotate parallel to the x-axis at higher temperatures. Since we actually measure the *in-plane* magnetization, not the total one, the mechanism just described may be responsible for the observed bump without violating the expected decreasing trend of the overall magnetic moment intensity.

As evident from the experimental data, the bump occurs in a range of temperatures where the bulk is almost paramagnetic. Therefore, the bulk critical temperature T_c^B must be lower than that of the special moments. If those were distributed throughout the bulk, like defects, the reciprocal coupling would be too weak to yield a Curie temperature higher than T_c^B. Hence, the special moments must form a magnetic system topologically separated from the bulk. A planar superficial distribution at the Ni/C interface is the most likely configuration; first, because the C-coating seems to play a crucial role; second, because other forms of aggregations inside the bulk (in the form of micro-domains) would result in the EH image as spots with attenuated (or absent) flux lines. Since T_c^B obviously falls in the neighborhood of the minimum of the temperature series in Fig. 3, we observe an increase of about 10% with respect to the value 627 K that is commonly taken as the Curie temperature in Nickel [18]. Such an increase is surprising for a relatively thick film such as ours. Initially we considered that the thermocouple reading the sample temperature was systematically in error. However, repeated testing on two samples with known magnetic transition temperatures (478 and 673 K) indicated that the nominal temperature reading of the stage control was accurate to within a degree or two. Furthermore, as discussed above, we carefully allowed for thermal equilibrium to be reached by waiting generous periods of time between temperature increments. Consequently, the increased T_c of our film, and the small but significant bump above the transition temperature cannot be easily dismissed. The high-temperature bump will be addressed in the next section; for now, we briefly turn our attention to the increased T_c that we observed experimentally.

While the observed T_c increase, in principle, could be related to magnetic impurities introduced during sample preparation, we can rule this possibility out on two grounds. First, during sample growth, the crucible holding the scientific grade Ni was pre-sputtered with the substrate shuttered from deposition in order to eliminate the possibility of cross-contamination between film growths in the UHV chamber. Examining the history of film growths in the chamber we used, the most likely candidate for sample contamination would be Fe. To increase T_c from the reference value by 10% to our observed value would require a film composition near $Ni_{94}Fe_6$. From a growth standpoint, this is unlikely. Secondly, to be sure, careful electron energy loss spectroscopy experiments were carried out on the same samples reported here. There was no observable Fe signal in the slightest, nor any observable signal from any other contaminant.

The increased T_c that we measure in our samples remains a mystery that we cannot easily explain. We can speculate, however, that the Carbon coating of our samples has produced some sort of structural changes that may be responsible for the observed T_c increase. In fact, the samples in this report were grown in the same exact conditions as the experiment reported in Ref. [19], where the observed critical temperature of 630 K was found very close indeed to the reference value, the only difference being the absence of any carbon-coating. While the coating might be responsible for the increased T_c, the available literature on the subject seems to contradict such explanation. Consequently, we are left with this currently unexplained experimental observation of an increased T_c.

In order to analyze the nature of the high-temperature bump that we observed experimentally, to which we now focus attention, we note that according to the standard micromagnetic framework, which we adopt for the remainder of the paper, the "spins" are intended as Heisenberg-type semi-classical elementary magnetic moments. Dimensionality, which in general is 3D for bulk crystalline Ni [20,21], is constrained to 3D-planar by the shape anisotropy typical of the thin foil geometry of our sample (including the presence of an edge that sets a preferential direction chosen as our x-axis). As for the actual size of each elementary moment in this framework, one may consider the fine polycrystalline nature of our sample, and take the average grain size (~ 10 nm) as a reference. However, the number of atoms, and hence the number N_{Bohr} of Bohr magnetons, participating in each micromagnetic moment, is an open question that may affect the validity of our semi-classical treatment. For large N_{Bohr}, the

classical picture is certainly appropriate, while the quantum picture is to be assumed if N_{Bohr} is of order of unity. Since the mean-field approximation adopted in the derivation of our interpretative model does not make a significant difference between the two cases, the micromagnetic framework in the semi-classical approximation has been chosen as the most convenient and flexible approach.

4. Theoretical model

As mentioned in Section 3, the model system that looks more appropriate for the description of the magnetization bump in Fig. 3 is a thin planar aggregate of special magnetic moments, aligned parallel to the z-axis at low temperature and rotating in the (x,y)-plane about the bulk Curie temperature T_c^B. We stress that at present the model is purely phenomenological and not supported by first principle calculations. However, it is possible to speculate about the physical origin of the underlying magnetic anisotropy, referring to other experimental observations and to other theories describing similar effects.

We did not find in the current literature direct evidence that the special magnetic moments lie at the interface between nickel and carbon. However, specific studies on the Ni/C surface [22] indicate that a structural phase transition, accompanied by carbon segregation, occurs at the nominal Curie temperature of Ni. This proves that the interface actually experiences strong mechanical and chemical modifications. In Ref. [22] it is suggested that those phenomena are related to a marked change of the electronic structure of Ni due to the presence of the segregated C-atoms. It is thereby possible that the magnetic properties do change accordingly. Studying this complex structure-property relationship by any conceivable analytical approach looks like a hard task. On the other hand, the topic may be fruitfully addressed by ab-initio numerical simulations that we plan to implement in the near future.

In pure Ni, T_c is an increasing function of the pressure [23], i.e., a decreasing function of the interatomic distance. Since we observe an increase of T_c^B, it is reasonable to think that carbon coating produces a contraction of the in-plane bonds forming the layers. This is consistent with the thermal expansion coefficient of carbon [24] $\alpha_C = 7.1$ ppm/K being about half that of nickel [24] $\alpha_{\mathrm{Ni}} \sim 13.7$ ppm/K (both values are quoted at room temperature, but it is reasonable to assume that their ratio remains similar at higher temperatures). If so, what one really should expect is a distribution of critical temperatures $T_c(z)$ such that closer to the Ni/C interface an increased contraction results in an increased T_c. In the simplest possible form, one can account for such features by introducing two Weiss domains: B (bulk) and I (interface), with elementary magnetic moments $\boldsymbol{\mu}^B$ and $\boldsymbol{\mu}^I$, and critical temperatures T_c^B and T_c^I respectively. Examples of a large enhancement of the Curie temperature at the surface with respect to the bulk value have been observed in Ni–Al solid solutions [25]. The bulk region contains the majority of the layers, while the interfacial region contains just the few layers in close contact with carbon. According to the argument outlined above, one expects that $T_c^B < T_c^I$. What precedes actually amounts to assume for $T_c(z)$ a stepwise function, changing abruptly at the border between I and B.

As outlined in the previous section, the bulk moments lie in the easy plane (x,y) of deposition mainly due to shape anisotropy. As far as the interface I is concerned, we assume that the mechanical and chemical modifications mentioned above result in an effect analogous to the so-called perpendicular surface anisotropy (PSA). PSA is the tendency of the magnetic moments of an ultra-thin film to align along the axis normal to the plane of deposition. In its standard formulation, PSA is due to the interplay between finite thickness (with critical upper limit) of the sample, and certain anisotropic exchange interactions [26] (in particular, spin–orbit coupling). This behavior has been observed in ultra-thin films of Ni and Co grown on nonmagnetic substrates (Pt and Au) [27,28]. It is worthwhile noticing that temperature dependent off-plane to in-plane transitions have been unambiguously observed by spin-polarized scanning electron microscopy in quasi-2D ferromagnetic systems [29]. In view of modeling the in-plane alignment of the interfacial moments at high temperatures, we have first exploited the possibility of a single-moment anisotropy, i.e. a potential energy well of finite depth, with minimum at $\theta = 0$, θ being the angle between $\boldsymbol{\mu}^I$ and the z-axis. This is the simplest way to construct an easy axis at low temperatures, with vanishing effect at higher temperatures, where the thermal energy exceeds the well's depth. However, since the in-plane alignment occurs incoherently in this case, the bump turns out to be too flat on the temperature scale, and is practically unobservable, no matter which model is assumed for the potential energy well.

For the in-plane alignment to be coherent, one has to introduce an anisotropy in the moment–moment interaction, such that the isotropic magnetic interaction energy density $j[\boldsymbol{\mu}^I(\mathbf{r}) \cdot \boldsymbol{\mu}^I(\mathbf{r}')]$ (proportional to the scalar product between the moments positioned at $\mathbf{r}, \mathbf{r}'$), is replaced by the more general tensorial expression

$$-\sum_{a,b=x,y,z} \mu_a^I(\mathbf{r})\mu_b^I(\mathbf{r}')j_{ab}^I. \tag{2}$$

It is worthwhile emphasizing the close analogy between Eq. (2) and the anisotropic term in Eq. (7) of Ref. [26], which is obtained from the PSA theory.

Here, we assume that the coupling tensor j_{ab}^I is diagonal, i.e. $j_{ab}^I = j_a^I \delta_{ab}$, but not proportional to the identity matrix (e.g., each j_a^I is different). In this case, a coherent in-plane alignment may occur, due to the cross-over between j_z^I and j_x^I at a certain temperature T_0. The effect turns out to be sharp on the temperature scale, even if the difference j_z^I-j_x^I approaches zero and changes sign very smoothly. The different temperature dependence of j_z^I and j_x^I is not surprising: indeed, the thermal expansion and the resulting decrease of j_z^I are expected to be more effective along the z-axis than in the x-direction, as a consequence of the assumed bond stiffening in the (x,y) plane due to the interface with carbon. For simplicity, we neglect the temperature dependence of j_x^I and write

$$j_z^I(T) = j_x^I\left[1 + \frac{T_0\text{-}T}{\Delta T} + \mathcal{O}([T\text{-}T_0]^2)\right]. \tag{3}$$

Eq. (3) is a standard linear expansion about the cross-over temperature T_0 at which $j_z^I(T_0) = j_x^I$. In summary, the bulk region B is described by an isotropic planar model in the (x,y) plane ($j_x^B = j_y^B = j^B$), and the interfacial region I by an anisotropic planar model in the (x,z) plane ($j_z^I \neq j_x^I$), with $j_z^I(T)$ depending on temperature according to Eq. (3).

For the moment, let us drop the indexes B and I, adopt the notation $\boldsymbol{\mu} = \mu\boldsymbol{\sigma}$, and refer to a general anisotropic planar model with normal axes labeled a and b. The resulting mean field (MF) anisotropic Hamiltonian (multiplied by $\beta = 1/KT$) for a single spin reads

$$h(\theta, \langle\boldsymbol{\sigma}\rangle) = \text{-}[2R_a\langle\sigma_a\rangle + r_a]\sigma_a\text{-}[2R_b\langle\sigma_b\rangle + r_b]\sigma_b, \tag{4}$$

where $2R_\eta = \beta\mu^2 j_\eta$; $r_\eta = \beta\mu B_\eta^{\mathrm{res}}; \eta = a, b$. In Eq. (4), the average components $\langle\sigma_\eta\rangle$ of the spin are the unknown quantities to be determined self-consistently. The factor of 2 in $2R_\eta$ is just for convenience. For a classical spin, one has $\sigma_a = \cos\theta, \sigma_b = \sin\theta$ and the self-consistent equations giving the equilibrium

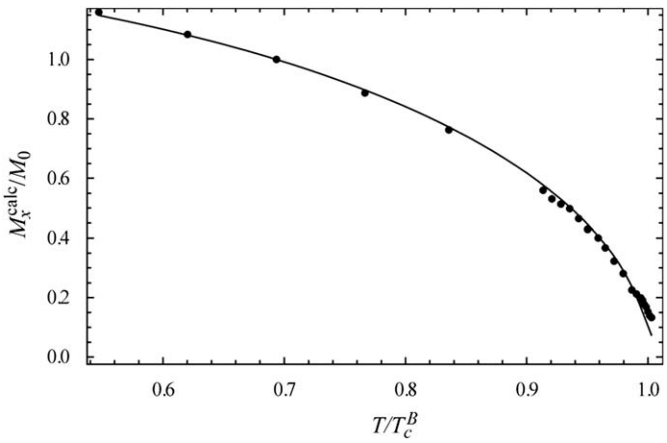

Fig. 4. Low temperature magnetization signal. The line is the best-fit curve for the magnetization. The errors on the experimental data are within the size of the points.

values are

$$\langle \sigma_a \rangle = Z^{-1} \int_0^{2\pi} \mathrm{d}\theta \cos\theta \exp[-h(\theta, \langle \boldsymbol{\sigma} \rangle)], \tag{5}$$

$$\langle \sigma_b \rangle = Z^{-1} \int_0^{2\pi} \mathrm{d}\theta \sin\theta \exp[-h(\theta, \langle \boldsymbol{\sigma} \rangle)], \tag{6}$$

where

$$Z = \int_0^{2\pi} \mathrm{d}\theta \exp[-h(\theta, \langle \boldsymbol{\sigma} \rangle)] \tag{7}$$

is the partition function of the system. After some elementary manipulations, one gets an equivalent system of equations in the A_η variables (where $A_\eta = 2R_\eta \langle \sigma_\eta \rangle + r_\eta$) that depend linearly on the averaged components of the spin as evidenced in Eq. (4):

$$A_\eta = \frac{2R_\eta A_\eta}{A} \phi(A) + r_\eta; \quad A = \sqrt{A_a^2 + A_b^2}; \tag{8}$$

$$\phi(A) = \frac{\mathrm{d}}{\mathrm{d}A} \log\left[\int_0^{2\pi} \mathrm{d}\theta \exp(A\cos\theta)\right]. \tag{9}$$

In the case $r_a = r_b = 0$, $R_a \neq R_b$ (anisotropic model without external fields), the system of Eqs. (8) and (9) has two sets of solutions: $A_a = 0, A_b = 2R_b\phi(A_b)$ (or the same with a and b interchanged). This means that the magnetic moments are oriented either along a or along b. The more stable orientation corresponds to the largest $|R_\eta|$, i.e., to the largest coupling. If $R_a = R_b = R$ (isotropic limit), it can be ascertained that $\langle \boldsymbol{\mu} \rangle$ is parallel to $\mathbf{r} = (r_a, r_b)$, i.e., to the residual field $\mathbf{B}^{\mathrm{res}}$.

For the bulk region one has $R_x^B = R_y^B = R^B$. Since $\mathbf{B}^{\mathrm{res}}$ has no component along y, the mean moment $\langle \boldsymbol{\mu}^B \rangle$ points in the x direction and is small for $T > T_c^B$, where the spontaneous magnetization vanishes.

The interfacial region, instead, displays a more complicated behavior. From the general argument discussed above, if $R_z^I(T)$-$R_x^I(T) \gg |r_{x,z}|$ the effects of the external fields are negligibly small, compared to the anisotropy, and $\langle \boldsymbol{\mu}^I \rangle$ is mainly directed along z. For the same reasons, $\langle \boldsymbol{\mu}^I \rangle$ is mainly directed along x if $R_x^I(T)$-$R_z^I(T) \gg |r_{x,z}|$. According to Eq. (3), the former case occurs for $T < T_0$ and the latter for $T > T_0$, provided T is not too close to T_0. In the neighborhood of the crossover temperature, in fact, there is a transition region where $|R_x^I(T)$-$R_z^I(T)| \approx |r_{x,z}|$. Here, the residual field is comparable to the anisotropy and determines the direction of $\langle \boldsymbol{\mu}^I \rangle$. Hence, the temperature-dependent anisotropy expressed by Eq. (3) makes $\langle \boldsymbol{\mu}^I \rangle$ rotate from the z direction to the x direction with increasing temperature, through a transition region. A schematic representation of the model and the spin reorientation transition occurring at the interface is shown in Fig. 5.

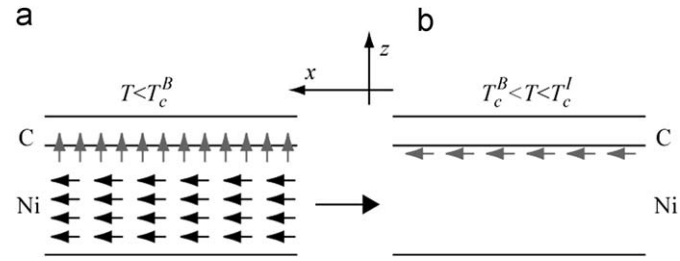

Fig. 5. Schematic view of the magnetic moments orientation at different temperatures: (a) low-temperature, where the interface moments are kept off-plane by perpendicular surface anisotropy; (b) high-temperature (above bulk Curie point), where the moment in the Ni film vanish, while the interface moments reorient themselves in-plane giving rise to the observed magnetization bump.

5. Comparison with experimental data

The calculated magnetization M_x^{calc} stems from solving the Eqs. (8) and (9) numerically for the two regions B and I, and summing the two contributions with an appropriate weight $\rho = N_I/N_B$, accounting for the different number of magnetic moments in the two regions. For simplicity, we assume $|\boldsymbol{\mu}^I| = |\boldsymbol{\mu}^B| = \mu$. This yields

$$M_x^{\mathrm{calc}} = M_0(\langle \sigma_x^B \rangle + \rho \langle \sigma_x^I \rangle). \tag{10}$$

Apart from the normalization constant M_0 (which can be chosen as the magnetization at a certain fixed temperature, e.g. $T = 473$ K), the best-fit parameters are $\rho, T_c^I, T_c^B, T_0, \Delta T, \mu$. Since it is reasonable to assume that the interfacial region between Ni and C is thin, the ratio ρ is expected to be small. The critical temperatures T_c^B, T_c^I and the cross-over temperature T_0 must satisfy the inequality $T_c^B < T_0 < T_c^I$ for the bump to be observable, and both must be comparable with the standard critical temperature $T_c = 627$ K for the model to make sense.

A preliminary estimate of ΔT and μ is not as easy due to the uncertainty on the number of Bohr magnetons contributing to each micromagnetic moment. In the expression $\mu = N_{\mathrm{Bohr}}\mu_{\mathrm{Bohr}}g/2$ giving the magnetic moment in terms of the Bohr magneton, the gyromagnetic factor $g = 1.92$ is known for Ni [18], while the number N_{Bohr} of Bohr magnetons is not.

While it is certain that ΔT^{-1} is proportional to the Ni thermal expansion coefficient α_{Ni}, calculating the proportionality factor would require a detailed knowledge of the electronic wave functions contributing the elementary magnetic moment, which includes the knowledge of N_{Bohr}. As a mere qualitative insight, one expects that ΔT^{-1} *increases* with the size of the units, since the moment–moment effective distance should be more sensitive to temperature changes, the larger the size.

At this stage, the best we can do is to choose some significant values of the number N_{Bohr} per micromagnetic moment, and best-fit the other parameters accordingly. The selected values are $N_{\mathrm{Bohr}} = 2, 5, 10, 20, 50, 100$. The results obtained are shown in Figs. 4 and 6. The best-fit values $\rho = 0.15$, $T_c^B = 682$ K, and $T_0 = 699$ K turn out to be independent on N_{Bohr}, while T_c^I displays a very weak, non monotonous dependence. In contrast, ΔT is strongly dependent on N_{Bohr} ($\Delta T \propto N_{\mathrm{Bohr}}^{-1}$), as shown in Table 1.

The low temperature behavior of $M_x^{\mathrm{calc}}(T)$ shown in Fig. 4 turns out to be almost insensitive to N_{Bohr}. Fig. 6 refers to $N_{\mathrm{Bohr}} = 5$ and shows a good agreement between calculated and measured

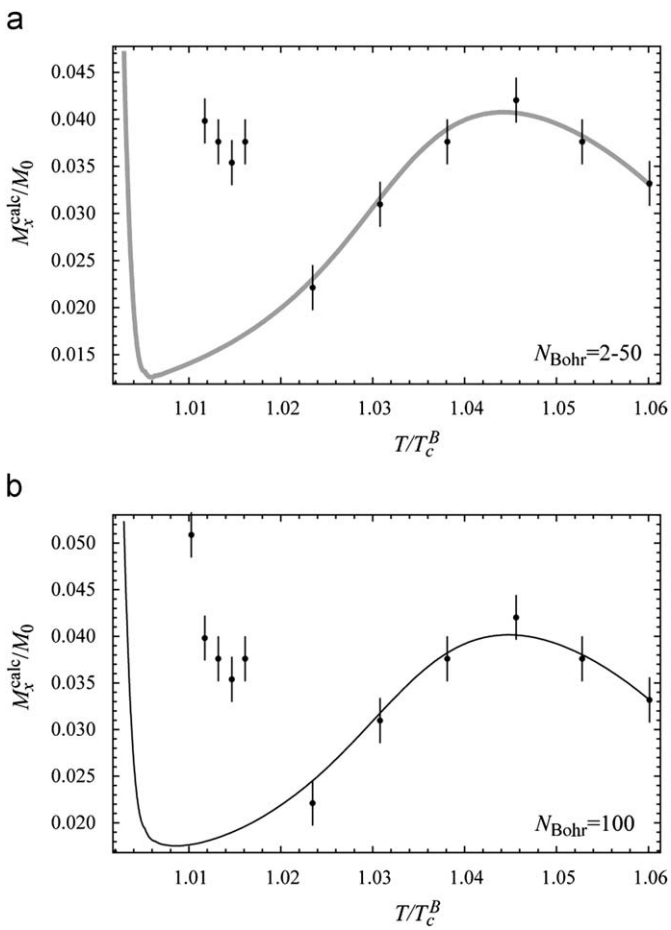

Fig. 6. High temperature signal and the observed bump. (a) The gray thick line contains all the five best-fit curves corresponding to $N_{Bohr} = 2, 5, 10, 20, 50$; (b) curve for $N_{Bohr} = 100$ that begins exceeding the experimental error bars.

Table 1
Best-fit results from the data, showing the very weak dependence of T_c^I on N_{Bohr} and the inverse proportionality between ΔT and N_{Bohr}.

N_{Bohr}	2	5	10	20	50	100
$T_c^{(I)}$ (K)	734.5	735.5	734.5	735.9	735.5	735.9
ΔT (10^6 K)	3.069	1.364	0.614	0.341	0.136	0.075

values from room temperature to about T_c^B. The curves for the other values of N_{Bohr} are indistinguishable within the range indicated, and have not been reported.

In the bump region $T > T_c^B$, the calculated $M_x^{calc}(T)$ displays in turn a weak dependence on N_{Bohr} for $N_{Bohr} = 2, 5, 10, 20, 50$ (and for all intermediate values). This can be seen from Fig. 6(a), in which the thickness of the gray line includes the five best-fit curves. The bump is very well reproduced, largely within the error bars. The value $N_{Bohr} = 100$, instead, is a limit case, above which the best-fit curves begin to exceed the error bars (Fig. 6(b)). Figs. 6(a) and (b) show that the model is not reliable about the minimum of $M_x^{calc}(T)$, just below the bump. In this small interval of temperatures, the calculated values systematically drop too steeply with respect to the measured values.

The preceding results indicate that the model reproduces the data very well except in the small transition region between the low temperature range, dominated by bulk region, and the high temperature range, dominated by the interfacial region. This may be due to three different reasons. First, the model neglects any possible B–I interaction, that should be relevant right in the intermediate region where $\langle \mu_x^I \rangle \simeq \langle \mu_x^B \rangle$. Indeed, the relatively small difference between the cross-over temperature $T_0 = 699$ K and the critical temperature $T_c^B = 682$ K is suggestive of some kind of magneto-elastic B–I interaction. Second, the present mean-field calculations cannot account exactly for the behavior of the B domain magnetization in the neighborhood of T_c^B, where renormalization group techniques would be required. Third, the present model is based on a stepwise picture of the critical temperature $T_c(z)$ of the layers, as a function of the distance from the Carbon coating layer. A more realistic smoother decrease from T_c^I to T_c^B would probably "fill in" the deep minimum displayed by the calculated magnetization just below the bump.

As a concluding remark, the weak dependence on N_{Bohr} of the calculated curves (Fig. 6) shows that the size of the elementary units carrying the magnetic moments is not relevant for the model's ability to reproduce the experimental data, at least for $N_{Bohr} < 100$. Such flexibility, however, is contingent upon the condition that ΔT in Eq. (3) varies with N_{Bohr} according to Table 1. It should be noticed that ΔT^{-1} increases almost linearly with N_{Bohr}, which supports the predicted increase with the size of the magnetic units [30,31]. The scarce dependence of the critical temperatures on N_{Bohr} is not surprising, given that we are fitting a set of data corresponding to *fixed* values of the Curie temperatures. What can be argued is that the effective moment-moment coupling between units containing N_{Bohr} magnetons decreases as N_{Bohr}^{-2} for T_c to be almost the same.

6. Conclusion

While attempting to assess the performance of EH in measuring the critical exponents of the ferromagnetic to paramagnetic transition, we have observed an unexpected increase in the magnetization above the nominal Curie temperature of a Nickel thin film coated with a thin layer of Carbon. The signal, in the form of a high-temperature "bump" is unequivocally significant, as EH, the technique we employed for the measurements, has sufficient sensitivity to detect it above noise and experimental uncertainties. It would be highly desirable if our holographic measurements were supported by different experimental techniques. This comparison, however, looks rather difficult, due to the small mass of the EH samples, that require a very high sensitivity of the probe, not accessible with standard vibrating sample magnetometers or differential scanning calorimeters. A possible alternative, superconducting quantum interferometer devices offer a high sensitivity and flexibility, but they can hardly operate above 100 °C, due to the difficulty of maintaining the superconducting state of the probe.

We interpret the signal as an effect of the perpendicular anisotropy present at the interface between the nickel film and carbon coating. More specifically, we describe the phenomenon as a strain-induced spin reorientation transition of the moments at the interface, off-plane at low temperature and in-plane at high temperature, due to the temperature dependence of their anisotropic exchange coupling constant. We presented a theoretical model capable of explaining the phenomenon within a mean-field approach. The model is based on a temperature dependent, moment–moment coupling anisotropy and accounts for the most relevant feature of the experimental signal, i.e. the clear separation, on the temperature scale, of the bump with respect to the bulk contribution. We showed that the model predictions are in excellent agreement with our observations. Our observations may be significant for understanding the complex interfacial phenomena occurring in strongly correlated multilayer thin films.

A puzzling aspect of the scenario we have explored is the $\sim 8\%$ increase of the bulk Curie temperature with respect to the reference value. Our measurement has been carried out by means of a model-dependent best-fit procedure within a mean-field approximation. One might wonder whether such an unexpected increase may be caused by the inadequacy of the model itself, and/or of the approximation used. We do not believe that this is the case, for two reasons: (i) the model for the bulk magnetization contains T_c^B as the unique free parameter, and there is practically no mixing with the other parameters characterizing the interface; (ii) the residual external field, determined with careful measurements in Ref. [12], is so small that any "smearing out" effect that might spoil the location of T_c^B, is to be considered quite negligible. In those conditions, we can take the best-fit value of T_c^B as a reliable expression for the real Curie temperature. The physical reasons for the increase of T_c^B are still unknown at the moment, and our current efforts are focusing on unraveling this mystery.

Acknowledgments

We gratefully acknowledge F. Boscherini and L. Pasquini for additional X-ray analysis of our samples, and L. Del Bianco for simulating discussions. Financial support was provided by the US Department of Energy, Basic Energy Sciences, under contract no. DE-AC02-98CH10886.

References

[1] A. Tonomura, Electron Holography, second ed., Springer, Berlin, 1999.
[2] D. Shindo, Y. Murakami, J. Phys. D Appl. Phys. 41 (2008) 183002.
[3] J.J. Kim, K. Hirata, Y. Ishida, D. Shindo, M. Takahashi, A. Tonomura, Appl. Phys. Lett. 92 (2008) 162501.
[4] A. Sugawara, H. Kasai, A. Tonomura, P.D. Brown, R.P. Campion, K.W. Edmonds, B.L. Gallagher, J. Zemen, T. Jungwirth, Phys. Rev. Lett. 100 (2008) 047202.
[5] M. Ammara, M. LoBue, E. Snoeck, M. Hÿtch, Y. Champion, R. Barrué, F. Mazaleyrat, J. Magn. Magn. Mat. 320 (2008) e716.
[6] F. Junginger, M. Kläui, D. Backes, S. Krzyk, U. Rüdiger, T. Kasama, R.E. Dunin-Borkowski, J.-M. Feinberge, R.J. Harrison, L.J. Heyderman, Appl. Phys. Lett. 92 (2008) 112502.
[7] J.M. Thomas, E.T. Simpson, T. Kasama, R.E. Dunin-Borkowski, Acc. Chem. Res. 41 (2008) 665.
[8] R.E. Dunin-Borkowski, M.R. McCartney, R.B. Frankel, D.A. Bazylinski, M. Pósfai, P.R. Buseck, Science 282 (1998) 1868.
[9] S.L. Tripp, R.E. Dunin-Borkowski, A. Wei, Angew. Chem. Int. Ed. 42 (2003) 5591.
[10] K. Yamamoto, S.A. Majetich, M.R. McCartney, M. Sachan, S. Yamamuro, T. Hirayama, Appl. Phys. Lett. 93 (2008) 082502.
[11] M.A. Schofield, M. Beleggia, G. Pozzi, Y. Zhu, Ultramicroscopy 108 (2008) 625.
[12] J.W. Lau, M.A. Schofield, Y. Zhu, Ultramicroscopy 107 (2007) 396.
[13] W. Dürr, M. Taborelli, O. Paul, R. Germar, W. Gaudat, D. Pescia, M. Landolt, Phys. Rev. Lett. 62 (1989) 206.
[14] Yi Li, M. Fürle, K. Baberscke, Phys. Rev. B—Rapid Commun. 41 (1990) 9596.
[15] C.A. Ballentine, R.L. Fink, J. Araya-Pochet, J.L. Erskine, Phys. Rev. B 41 (1990) 2631.
[16] E. Völkl, L. Allard, D.C. Joy, Introduction to Electron Holography, Kluwer Academics, Dordrecht, 1999.
[17] M.A. Schofield, unpublished algorithm.
[18] C. Kittel, Introduction to Solid State Physics, Wiley, New York, 1996.
[19] G. Matteucci, Philos. Mag. Lett. 86 (2006) 81.
[20] T.A. Kachnowski, R.M. Suter, A.M. Gottlieb, C. Hoenemser, Phys. Rev. B 14 (1976) 5022.
[21] N. Stüsser, M.Th. Rekveldt, T. Spruijt, Phys. Rev. B 33 (1986) 6423.
[22] J.C. Hamilton, T. Jach, Phys. Rev. Lett. 46 (1981) 745.
[23] K.P. Belov, Magnetic Transition, Consultant Bureau, New York, 1961, p. 101, Table 8.
[24] WebElements: the periodic table on the web, 〈http://www.webelements.com/physics.html〉.
[25] M. Polak, L. Rubinovich, J. Deng, Phys Rev. Lett. 74 (1995) 4059.
[26] S. Zhang, Phys. Rev. B 45 (1992) 7487.
[27] B.N. Engel, M.H. Wiedmann, R.A. Van Leeuwen, C.M. Falco, Phys. Rev. B 48 (1993) 9894.
[28] B. Ujfalussy, L. Szunyogh, P. Bruno, P. Weinberger, Phys. Rev. Lett. 77 (1996) 1805.
[29] R. Allenspach, A. Bischof, Phys. Rev. Lett. 69 (1992) 3385.
[30] S.E. Apsel, J.W. Emmert, J. Deng, L.A. Bloomfield, Phys. Rev. Lett. 76 (1996) 1441.
[31] N. Fujima, T. Yamaguchi, Phys. Rev. B 54 (1996) 26.